science.sciencemag.org/cgi/content/full/science.abb7269/DC1

Supplementary Materials for

A highly conserved cryptic epitope in the receptor-binding domains of SARS-CoV-2 and SARS-CoV

Meng Yuan*, Nicholas C. Wu*, Xueyong Zhu, Chang-Chun D. Lee, Ray T. Y. So, Huibin Lv, Chris K. P. Mok†, Ian A. Wilson†

*These authors contributed equally to this work.
†Corresponding author. Email: ch02mkp@hku.hk (C.K.P.M.); wilson@scripps.edu (I.A.W.)

Published 3 April 2020 on *Science* First Release
DOI: 10.1126/science.abb7269

This PDF file includes:

Other Supplementary Material for this manuscript includes the following:
(available at science.sciencemag.org/cgi/content/full/science.abb7269/DC1)

MDAR Reproducibility Checklist (.pdf)

This PDF file includes:

Materials and Methods

Figs. S1 to S6

Tables S1 to S3

References 37-46

MATERIALS AND METHODS

Expression and purification of RBD

The receptor-binding domain (RBD) (residues 319-541) of the SARS-CoV-2 spike (S) protein (GenBank: QHD43416.1), as well as the RBD (residues 306-527) of the SARS-CoV S protein (GenBank: ABF65836.1), were cloned into a customized pFastBac vector (*37*). The RBD constructs were fused with an N-terminal gp67 signal peptide and a C-terminal His_6 tag. Recombinant bacmid DNA was generated using the Bac-to-Bac system (Life Technologies). Baculovirus was generated by transfecting purified bacmid DNA into Sf9 cells using FuGENE HD (Promega), and subsequently used to infect suspension cultures of High Five cells (Life Technologies) at an MOI of 5 to 10. Infected High Five cells were incubated at 28 °C with shaking at 110 r.p.m. for 72 h for protein expression. The supernatant was then concentrated using a 10 kDa MW cutoff Centramate cassette (Pall Corporation). The S and RBD proteins were purified by Ni-NTA, followed by size exclusion chromatography, and buffer exchanged into 20 mM Tris-HCl pH 7.4 and 150 mM NaCl.

Expression and purification of CR3022 Fab and IgG

The CR3022 Fab heavy (GenBank: DQ168569.1) and light (GenBank: DQ168570.1) chains were cloned into phCMV3. The plasmids were transiently co-transfected into Expi293F cells at a ratio of 2:1 (HC:LC) using ExpiFectamine™ 293 Reagent (Thermo

Fisher Scientific) according to the manufacturer's instructions. The supernatant was collected at 7 days post-transfection. The Fab was purified with a CaptureSelect™ CH1-XL Pre-packed Column (Thermo Fisher Scientific) followed by size exclusion chromatography.

For full-length IgGs of CR3022, m396 (sequences from PDB 2DD8 (*16*)), and S230.15 (sequences from PDB 6NB6 (*38*)), the heavy-chain and light-chain plasmids were transiently co-transfected into ExpiCHO cells at a ratio of 2:1 using ExpiFectamine™ CHO Reagent (Thermo Fisher Scientific) according to the manufacturer's instructions. The supernatant was collected at 14 days post-transfection. The IgGs were purified using a Protein G column (GE Healthcare), and further purified by size exclusion chromatography.

Crystallization and structural determination

Purified CR3022 Fab and SARS-CoV-2 RBD were mixed at a molar ratio of 1:1 and incubated overnight at 4 °C. The complex (15 mg/ml) was screened for crystallization using the 384 conditions of the JCSG Core Suite (Qiagen) at 293 K on our custom-designed robotic CrystalMation system (Rigaku) at Scripps Research by the vapor diffusion method in sitting drops containing 0.1 µl of protein and 0.1 µl of reservoir solution. Optimized crystals were then grown in 80 mM sodium acetate pH 4.6, 1.5 M ammonium sulfate, and 20% glycerol. Crystals were grown for 14 days and then flash cooled in liquid nitrogen. Diffraction data were collected at cryogenic temperature (100 K) at beamline 23-ID-D of the Argonne Photon Source (APS) with a beam wavelength of 1.033 Å, and processed with HKL2000 (*39*). Structures were solved by molecular replacement using PHASER with homology models for Fab CR3022 generated from PDB ID: 4KMT (*40*) and for SARS-CoV-2 RBD generated from a structure of SARS-

CoV-RBD (PDB ID: 2AJF) (*41*) with SWISS-MODEL (*42*). Iterative model building and refinement were carried out in COOT (*43*) and PHENIX (*44*), respectively. Epitope and paratope residues, as well as their interactions, were identified by accessing PISA at the European Bioinformatics Institute (http://www.ebi.ac.uk/pdbe/prot_int/pistart.html) (*34*).

Biolayer interferometry binding assay

Binding assays were performed by biolayer interferometry (BLI) using an Octet Red instrument (FortéBio) as described previously (*45*). Briefly, His_6-tagged S and RBD proteins at 20 to 100 µg/mL in 1x kinetics buffer (1x PBS, pH 7.4, 0.01% BSA and 0.002% Tween 20) were loaded onto Anti-Penta-HIS (HIS1K) biosensors and incubated with the indicated concentrations of CR3022 Fab or IgG. The assay consisted of five steps: 1) baseline: 60 s with 1x kinetics buffer; 2) loading: 300 s with his_6-tagged S or RBD proteins; 3) baseline: 60 s with 1x kinetics buffer; 4) association: 120 s with samples (Fab or IgG); and 5) dissociation: 120 s with 1x kinetics buffer. For estimating the exact K_d, a 1:1 binding model was used.

Microneutralization assay

Monoclonal antibodies were mixed with equal volumes of SARS-CoV or SARS-CoV-2 at a dose of 100 tissue culture infective doses 50% ($TCID_{50}$) determined by Vero and Vero E6 cells respectively. After 1 hour of incubation at 37°C, 35 µl of the virus-antibody mixture was added in quadruplicate to Vero or Vero E6 cell monolayers in 96-well microtiter plates. After 1 hour of adsorption, the virus-antibody mixture was removed and replaced with 150 µl of virus growth medium in each well. The plates were incubated for 3 days at 37°C in 5% CO_2 in a humidified incubator. A cytopathic effect was observed at day 3 post-inoculation. The highest plasma dilution that protected 50% of the replicate

wells was denoted as the neutralizing antibody titer. A virus back-titration of the input virus was included in each batch of tests.

ELISA binding assay to virus and RBD

96-well enzyme-linked immunosorbent assay (ELISA) plates (Nunc MaxiSorp, Thermo Fisher Scientific) were first coated overnight with 10^5 $TCID_{50}$ SARS-CoV-2 or SARS-CoV or 100 ng of purified recombinant RBD protein of the two viruses per well in PBS buffer. The plates coated with either virus or protein were then blocked with PBS containing 5% non-fat milk powder at room temperature for 2 hours. 100 µl of CR3022 or m396 at a concentration of 200 µg/ml was added to the ELISA wells with different coating condition for 2-hour incubation at 37°C. After extensive washing with PBS containing 0.1% Tween 20, HRP-conjugated goat anti-human IgG (1:5000, GE Healthcare) was added for 1 hour at 37°C. The ELISA plates were then washed five times with PBS containing 0.1% Tween 20. Subsequently, 100 µl of HRP substrate (TMB One) (New Cell & Molecular Biotech) was added into each well. After 20 minutes incubation, the reaction was stopped by adding 50 µl of 2 M H_2SO_4 solution and analyzed on a Sunrise absorbance microplate reader (Tecan) at 450 nm wavelength. The normalized results were obtained by the calculating the difference between the OD of the purified recombinant protein-coated well and the PBS-coated well.

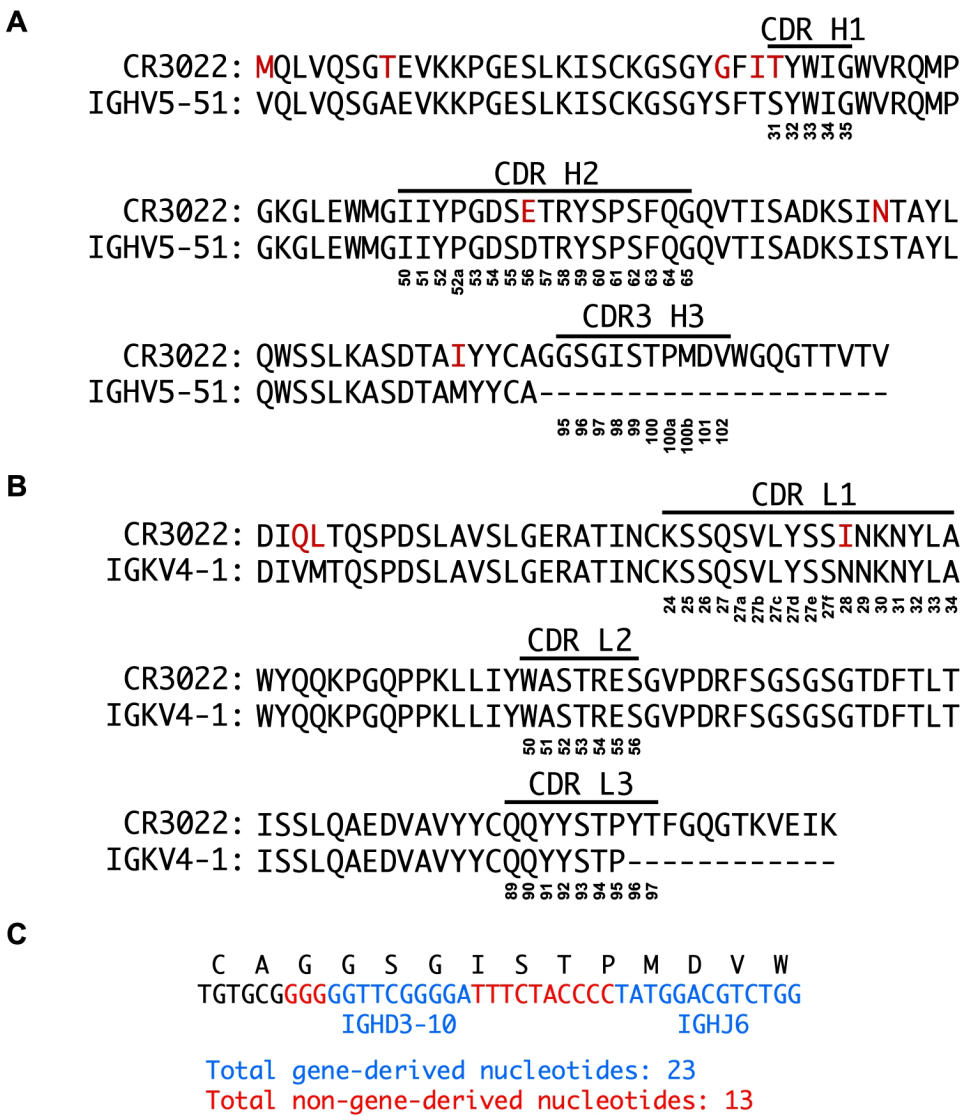

Fig. S1. Comparison of CR3022 sequence to its putative germline sequence. Alignment of CR3022 **(A)** with the germline IGHV5-51 sequence, and **(B)** with the germline IGKV4-1 sequence. The regions that correspond to CDR H1, H2, H3, L1, L2, and L3 are indicated. Residues that differ from the germline are highlighted in red. Residue positions in the CDRs are labeled according to the Kabat numbering scheme. **(C)** Sequence of the V-D-J junction of CR3022, with putative gene segments (blue) and N-regions (red), are indicated.

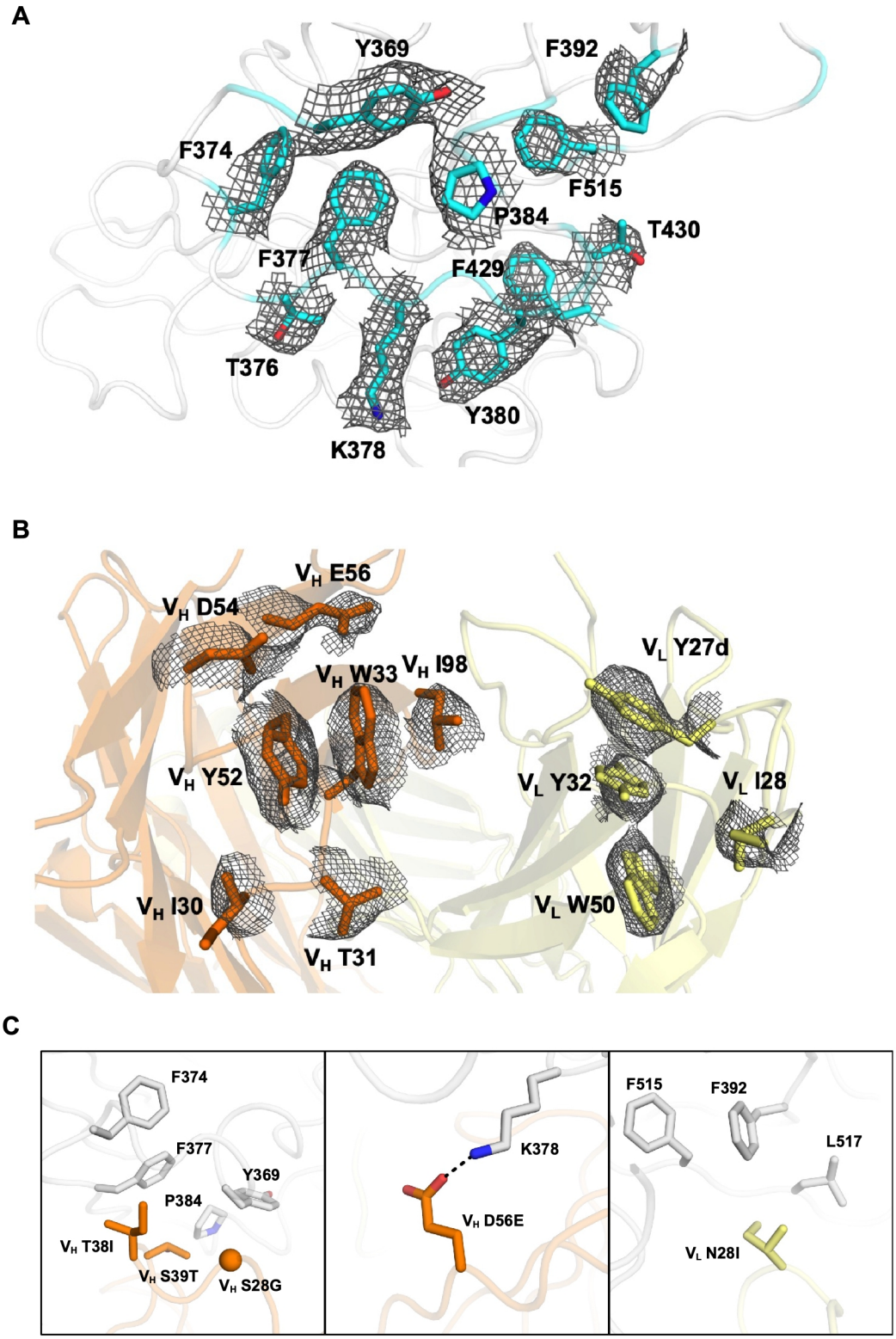

127

128 **Fig. S2. Electron density maps for epitope and paratope regions and structural**

analysis of somatic mutations. (A) Final 2Fo-Fc electron density maps for the side chains in the epitope region (cyan) of SARS-CoV-2 contoured at 1 σ. **(B)** Final 2Fo-Fc electron density maps for the paratope region of CR3022 contoured at 1 σ. The heavy chain is colored in orange, and light chain in yellow. Residues are labeled. **(C)** Somatic mutations V_H S28G, V_H T38I, V_H S39T, V_H D56E, and V_L N28I are located in the CR3022 paratope region. Hydrogen bonds are represented by dashed lines. CR3022 heavy chain is in orange and light chain is in yellow. SARS-CoV-2 RBD is in light grey.

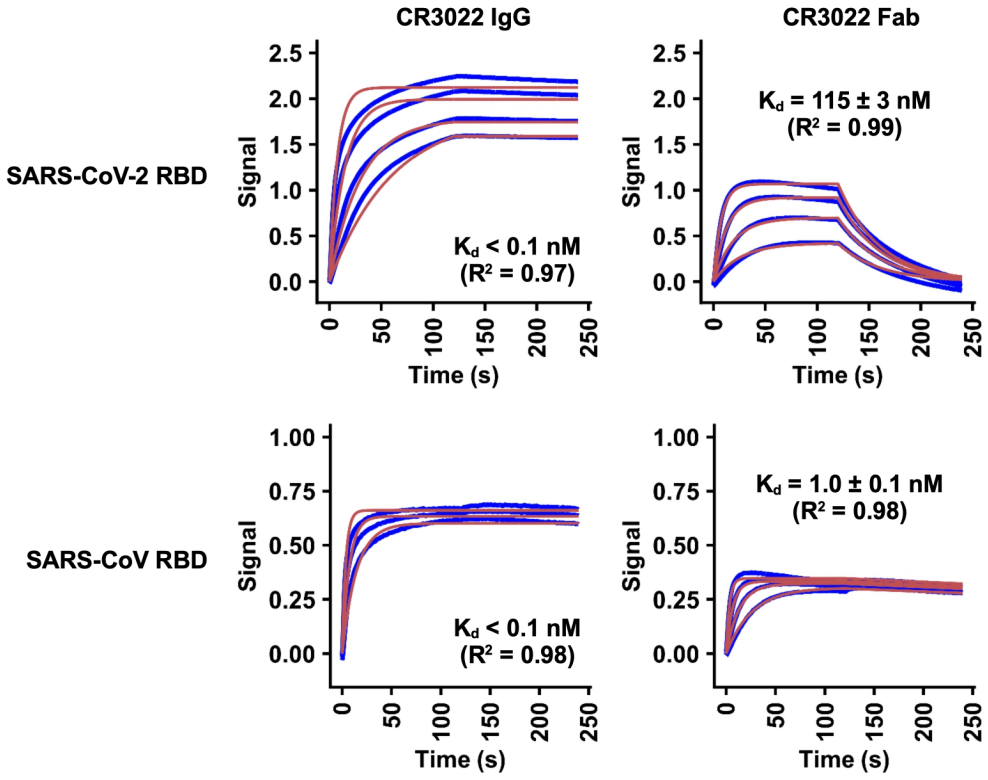

Fig. S3. Sensorgrams for binding of CR3022 IgG and Fab to RBDs of SARS-CoV-2 and SARS-CoV. Binding kinetics of CR3022 Fab and IgG against the RBDs of SARS-CoV-2 and SARS-CoV were measured by biolayer interferometry (BLI). Y-axis represents the response. Blue lines represent the response curves and red lines represent the 1:1 binding model. Binding kinetics were measured for three to four concentrations of IgG or Fab at 2-fold dilution ranging from 500 nM to 62.5 nM. The K_d and R^2 of the fitting are indicated. The enhanced binding of IgG as compared to Fab is likely due to bivalent binding. Of note, stoichiometry cannot be inferred from this experiment. Previously, Tian et al. (*6*) reported a K_d of 6 nM between CR3022 and SARS-CoV-2 RBD. However, there are several differences between the two experiments. Firstly, CR3022 was expressed as single-chain fragment variable (scFv) in Tian et al. (*6*), but as an Fab in our study. Secondly, CR3022 was expressed in *E. coli* in Tian et al. (*6*), but in mammalian cells in our study. Thirdly, SARS-CoV-2 RBD was

expressed in mammalian cells in Tian et al. (*6*), but in insect cells in our study.

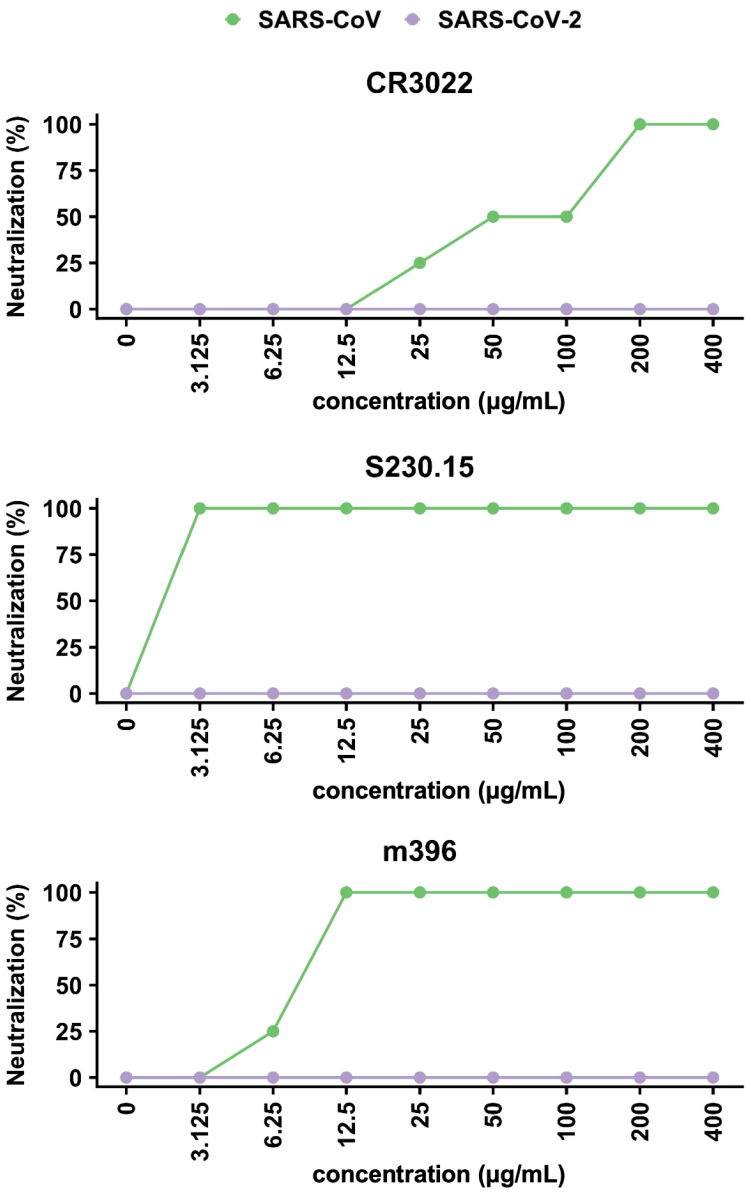

Fig. S4. Neutralization activity of SARS-neutralizing monoclonal antibodies against SARS-CoV-2 and SARS-CoV. Microneutralization of SARS-CoV-2 and SARS-CoV with monoclonal antibodies **(A)** CR3022 (*4*), **(B)** S230.15 (*38*), and **(C)** m396 (*16*). Neutralization of 100 $TCID_{50}$ of each virus was performed in quadruplicate. S230.15 and m396 are SARS-CoV-specific antibodies that do not cross-react with SARS-CoV-2 (*6, 17*).

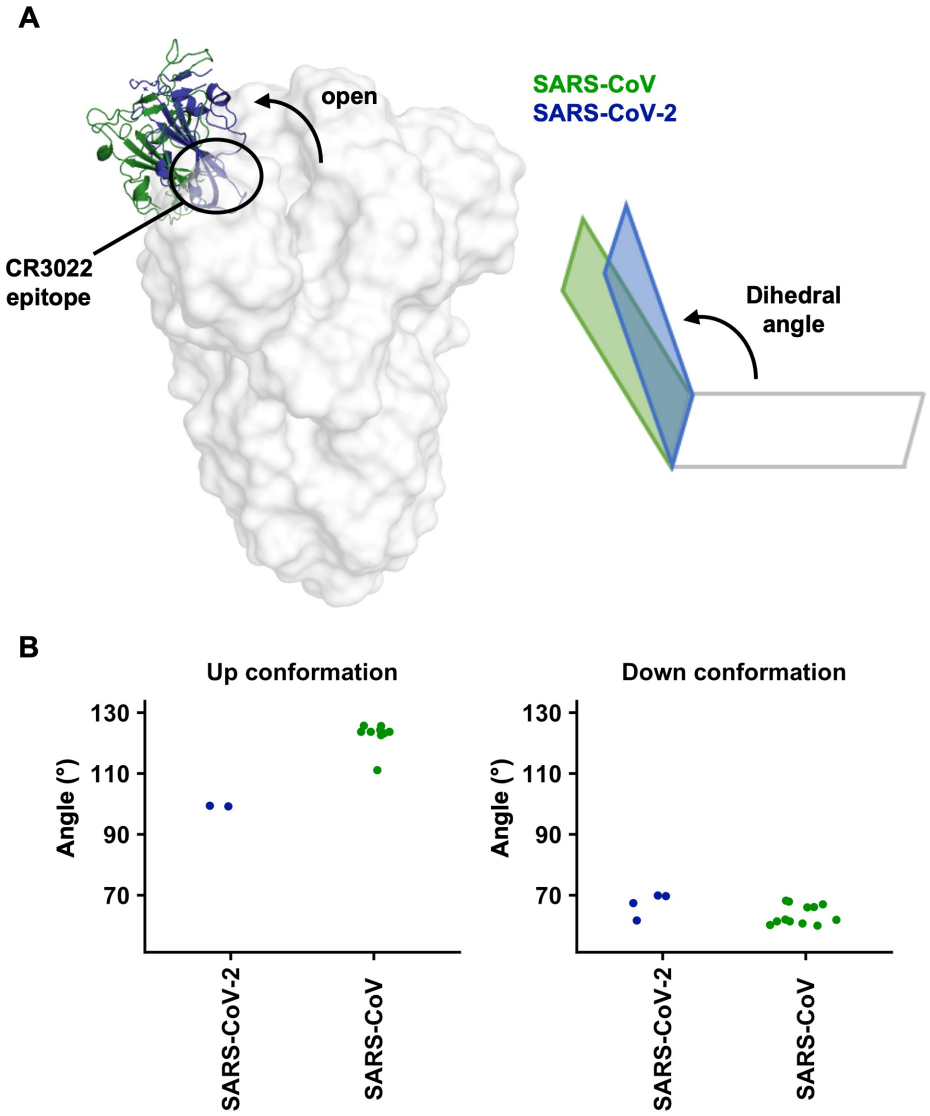

C

PDB	2AJF (copy 1)	2AJF (copy 2)	6VSB (protomer 1)	6VSB (protomer 2)	6VSB (protomer 3)	6VYB (protomer 1)	6VYB (protomer 2)	6VYB (protomer 3)
State	-	-	up	down	down	up	down	down
RMSD (Å)	1.22	1.54	1.11	1.94	1.00	1.07	1.37	1.11

Fig. S5. Comparison of the "up" conformations between the SARS-CoV-2 and SARS-CoV S proteins. (A) Structural alignment of the one-"up" S proteins from SARS-CoV-2 (PDB 6VSB (*17*)) and SARS-CoV (PDB 6CRW (*21*)). The RBD with an "up"

conformation from SARS-CoV-2 is in blue and from SARS-CoV is in green. **(B)** The RBD open angle is represented by a dihedral angle between the RBD and the horizontal plane. Given that the RBD of interest is on protomer 1, the dihedral angle is measured by the angle of P507 Cα (protomer 1) – R983 Cα (protomer 2) – R983 Cα (protomer 1) – R983 Cα (protomer 3) for SARS-CoV-2, which corresponds to of P493 Cα (protomer 1) – R965 Cα (protomer 2) – R965 Cα (protomer 1) – R965 Cα (protomer 3) for SARS-CoV. For this analysis, S protein structures with PDB IDs of 6VSB (*17*), 6VYB (*18*) were used for SARS-CoV-2, whereas 5X5B (*19*), 6CRX (*21*), 6CS0, 6CS1, 6CRW (*21*), 6ACD (*46*), and 6CRZ (*21*) were used for SARS-CoV. **(C)** Root-mean-square deviation (RMSD Cα) of the RBDs from different structures were computed using “super” function in PyMOL with no refinement cycle. PDB 2AJF (*41*), 6VSB (*17*), and 6VYB (*18*) were used in this analysis.

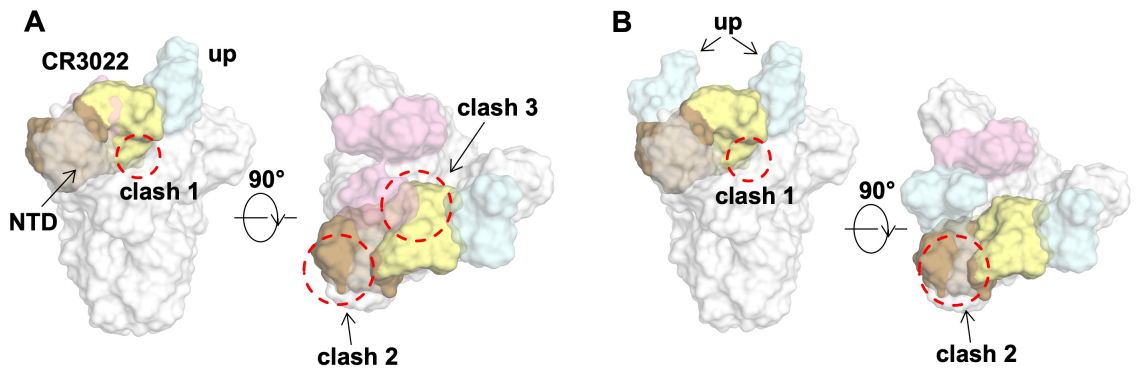

Fig. S6. Modeling of the binding of CR3022 to the homotrimeric SARS-CoV S protein. Same as panels D and E in Fig. 4, except that the S protein from SARS-CoV was used for modeling compared to SARS-CoV-2 in Fig. 4. **(A)** Binding of CR3022 to single-"up" configuration would clash (indicated by the red circles) with the S protein. Clash 1: CR3022 variable region clashes with the S2 subunit. Clash 2: CR3022 constant region clashes with NTD. Clash 3: CR3022 variable region clashes with the neighboring RBD that is in "down" conformation. CR3022 variable region is colored yellow. CR3022 constant region is colored brown. RBD in "up" conformation is colored cyan. RBD in "down" conformation is colored pink. PDB 6CRW is used as a model for the single-"up" configuration of SARS-CoV S protein (*21*). **(B)** Clash 3 can be resolved when the neighboring RBD is in "up" conformation (i.e. S protein in double-"up" configuration). PDB 6CRX is used a model for the double-"up" configuration of SARS-CoV S protein (*21*).

Table S1. X-ray data collection and refinement statistics

Data collection	
Beamline	APS 23ID-D
Wavelength (Å)	1.03322
Space group	$P4_122$
Unit cell parameters	a=b=147.5°, c=200.2°
Resolution (Å)	50.0-3.10 (3.21-3.10)[a]
Unique reflections	41,206 (938)[a]
Redundancy	6.7 (5.5)[a]
Completeness (%)	100.0 (100.0)[a]
$\langle I/\sigma_I \rangle$	18.8 (1.0)[a]
R_{sym}[b] (%)	13.6 (>100)[a]
R_{pim}[b] (%)	4.0 (54.0)[a]
$CC_{1/2}$[c] (%)	100.0 (59.1)[a]
Refinement statistics	
Resolution (Å)	50.0-3.10
Reflections (work)	41,137
Reflections (test)	2,030
R_{cryst}[d] / R_{free}[e] (%)	22.3/24.3
No. of atoms	4,936
Macromolecules	4,906
Ligands	30
Average *B*-value (Å^2)	99
Macromolecules	99
Ligands	137
Wilson *B*-value (Å^2)	95
RMSD from ideal geometry	
Bond length (Å)	0.002
Bond angle (°)	0.52
Ramachandran statistics (%)	
Favored	97.2
Outliers	0.0
PDB code	6W41

[a] Numbers in parentheses refer to the highest resolution shell.

[b] $R_{sym} = \Sigma_{hkl} \Sigma_i | I_{hkl,i} - \langle I_{hkl} \rangle | / \Sigma_{hkl} \Sigma_i I_{hkl,i}$ and $R_{pim} = \Sigma_{hkl} (1/(n-1))^{1/2} \Sigma_i | I_{hkl,i} - \langle I_{hkl} \rangle | / \Sigma_{hkl} \Sigma_i I_{hkl,i}$, where $I_{hkl,i}$ is the scaled intensity of the ith measurement of reflection h, k, l, $\langle I_{hkl} \rangle$ is the average intensity for that reflection, and *n* is the redundancy.

[c] $CC_{1/2}$ = Pearson correlation coefficient between two random half datasets.

[d] $R_{cryst} = \Sigma_{hkl} | F_o - F_c | / \Sigma_{hkl} | F_o | \times 100$, where F_o and F_c are the observed and calculated structure factors, respectively.

[e] R_{free} was calculated as for R_{cryst}, but on a test set comprising 5% of the data excluded from refinement.

191

Table S2. Hydrogen bonds and salt bridges identified at the SARS-CoV-2 RBD and CR3022 interface using the PISA program

Hydrogen bonds		
SARS-CoV-2 RBD	**Dist. (Å)**	**CR3022**
PHE377[N]	3.0	V_H TYR52[OH]
LYS378[N]	3.9	V_H TYR52[OH]
LYS378[NZ]	2.7	V_H ASP54[OD2]
LYS378[NZ]	2.4	V_H GLU56[OE1]
LYS386[NZ]	3.3	V_H ASP101[OD1]
PHE377[O]	2.5	V_H TYR52[OH]
CYS379[O]	3.2	V_H ILE98[N]
THR430[OG1]	2.4	V_L SER27f[OG]
GLY381[O]	2.3	V_L TYR32[OH]
Salt bridges		
LYS378[NZ]	2.7	V_H ASP54[OD2]
LYS378[NZ]	2.4	V_H GLU56[OE1]
LYS378[NZ]	3.4	V_H ASP54[OD1]
LYS386[NZ]	3.3	V_H ASP101[OD1]
LYS386[NZ]	3.6	V_H ASP101[OD2]

197 **Table S3. Epitope residues on the SARS-CoV-2 RBD and**
198 **their buried surface area upon binding to CR3022**
199

200

201

SARS-CoV-2 RBD	BSA (Å^2)
TYR369	50
ASN370	41
SER371	5
ALA372	11
PHE374	17
SER375	17
THR376	23
PHE377	63
LYS378	96
CYS379	35
TYR380	66
GLY381	11
VAL382	8
SER383	37
PRO384	33
THR385	42
LYS386	105
ASP389	6
LEU390	32
PHE392	17
ASP427	7
ASP428	58
PHE429	7
THR430	50
PHE515	6
GLU516	6
LEU517	49
HIS519	20

References and Notes

1. C. Huang, Y. Wang, X. Li, L. Ren, J. Zhao, Y. Hu, L. Zhang, G. Fan, J. Xu, X. Gu, Z. Cheng, T. Yu, J. Xia, Y. Wei, W. Wu, X. Xie, W. Yin, H. Li, M. Liu, Y. Xiao, H. Gao, L. Guo, J. Xie, G. Wang, R. Jiang, Z. Gao, Q. Jin, J. Wang, B. Cao, Clinical features of patients infected with 2019 novel coronavirus in Wuhan, China. *Lancet* **395**, 497–506 (2020). doi:10.1016/S0140-6736(20)30183-5 Medline

2. Coronaviridae Study Group of the International Committee on Taxonomy of Viruses, The species Severe acute respiratory syndrome-related coronavirus: Classifying 2019-nCoV and naming it SARS-CoV-2. *Nat. Microbiol.* **5**, 536–544 (2020). doi:10.1038/s41564-020-0695-z Medline

3. P. Zhou, X.-L. Yang, X.-G. Wang, B. Hu, L. Zhang, W. Zhang, H.-R. Si, Y. Zhu, B. Li, C.-L. Huang, H.-D. Chen, J. Chen, Y. Luo, H. Guo, R.-D. Jiang, M.-Q. Liu, Y. Chen, X.-R. Shen, X. Wang, X.-S. Zheng, K. Zhao, Q.-J. Chen, F. Deng, L.-L. Liu, B. Yan, F.-X. Zhan, Y.-Y. Wang, G.-F. Xiao, Z.-L. Shi, A pneumonia outbreak associated with a new coronavirus of probable bat origin. *Nature* **579**, 270–273 (2020). doi:10.1038/s41586-020-2012-7 Medline

4. J. ter Meulen, E. N. van den Brink, L. L. M. Poon, W. E. Marissen, C. S. W. Leung, F. Cox, C. Y. Cheung, A. Q. Bakker, J. A. Bogaards, E. van Deventer, W. Preiser, H. W. Doerr, V. T. Chow, J. de Kruif, J. S. M. Peiris, J. Goudsmit, Human monoclonal antibody combination against SARS coronavirus: Synergy and coverage of escape mutants. *PLOS Med.* **3**, e237 (2006). doi:10.1371/journal.pmed.0030237 Medline

5. J. Ye, N. Ma, T. L. Madden, J. M. Ostell, IgBLAST: An immunoglobulin variable domain sequence analysis tool. *Nucleic Acids Res.* **41**, W34–W40 (2013). doi:10.1093/nar/gkt382 Medline

6. X. Tian, C. Li, A. Huang, S. Xia, S. Lu, Z. Shi, L. Lu, S. Jiang, Z. Yang, Y. Wu, T. Ying, Potent binding of 2019 novel coronavirus spike protein by a SARS coronavirus-specific human monoclonal antibody. *Emerg. Microbes Infect.* **9**, 382–385 (2020). doi:10.1080/22221751.2020.1729069 Medline

7. See supplementary materials.

8. Y. Watanabe, Z. T. Berndsen, J. Raghwani, G. E. Seabright, J. D. Allen, J. S. McLellan, I. A. Wilson, T. A. Bowden, A. B. Ward, M. Crispin, Vulnerabilities in coronavirus glycan shields despite extensive glycosylation. bioRxiv 2020.02.20.957472 [Preprint]. 21 February 2020. https://doi.org/10.1101/2020.02.20.957472.

9. M. Letko, A. Marzi, V. Munster, Functional assessment of cell entry and receptor usage for SARS-CoV-2 and other lineage B betacoronaviruses. *Nat. Microbiol.* **5**, 562–569 (2020). doi:10.1038/s41564-020-0688-y Medline

10. R. Yan, Y. Zhang, Y. Li, L. Xia, Y. Guo, Q. Zhou, Structural basis for the recognition of SARS-CoV-2 by full-length human ACE2. *Science* **367**, 1444–1448 (2020). doi:10.1126/science.abb2762 Medline

11. J. Lan, J. Ge, J. Yu, S. Shan, H. Zhou, S. Fan, Q. Zhang, X. Shi, Q. Wang, L. Zhang, X. Wang, Crystal structure of the 2019-nCoV spike receptor-binding domain bound with the ACE2 receptor. bioRxiv 2020.02.19.956235 [Preprint]. 20 February 2020. https://doi.org/10.1101/2020.02.19.956235.

12. ACE2 also forms a dimer when it associates with an amino acid transporter B0AT1 (*10*). We modeled a CR3022 IgG onto this dimer structure and found no clashes of CR3022 with ACE2 in its dimeric form where the RBDs would likely come from adjacent trimers on the virus (*10*).

13. J. Sui, W. Li, A. Murakami, A. Tamin, L. J. Matthews, S. K. Wong, M. J. Moore, A. S. C. Tallarico, M. Olurinde, H. Choe, L. J. Anderson, W. J. Bellini, M. Farzan, W. A. Marasco, Potent neutralization of severe acute respiratory syndrome (SARS) coronavirus by a human mAb to S1 protein that blocks receptor association. *Proc. Natl. Acad. Sci. U.S.A.* **101**, 2536–2541 (2004). doi:10.1073/pnas.0307140101 Medline

14. E. N. van den Brink, J. Ter Meulen, F. Cox, M. A. C. Jongeneelen, A. Thijsse, M. Throsby, W. E. Marissen, P. M. L. Rood, A. B. H. Bakker, H. R. Gelderblom, B. E. Martina, A. D. M. E. Osterhaus, W. Preiser, H. W. Doerr, J. de Kruif, J. Goudsmit, Molecular and biological characterization of human monoclonal antibodies binding to the spike and nucleocapsid proteins of severe acute respiratory syndrome coronavirus. *J. Virol.* **79**, 1635–1644 (2005). doi:10.1128/JVI.79.3.1635-1644.2005 Medline

15. J. D. Berry, S. Jones, M. A. Drebot, A. Andonov, M. Sabara, X. Y. Yuan, H. Weingartl, L. Fernando, P. Marszal, J. Gren, B. Nicolas, M. Andonova, F. Ranada, M. J. Gubbins, T. B. Ball, P. Kitching, Y. Li, A. Kabani, F. Plummer, Development and characterisation of neutralising monoclonal antibody to the SARS-coronavirus. *J. Virol. Methods* **120**, 87–96 (2004). doi:10.1016/j.jviromet.2004.04.009 Medline

16. P. Prabakaran, J. Gan, Y. Feng, Z. Zhu, V. Choudhry, X. Xiao, X. Ji, D. S. Dimitrov, Structure of severe acute respiratory syndrome coronavirus receptor-binding domain complexed with neutralizing antibody. *J. Biol. Chem.* **281**, 15829–15836 (2006). doi:10.1074/jbc.M600697200 Medline

17. D. Wrapp, N. Wang, K. S. Corbett, J. A. Goldsmith, C.-L. Hsieh, O. Abiona, B. S. Graham, J. S. McLellan, Cryo-EM structure of the 2019-nCoV spike in the prefusion conformation. *Science* **367**, 1260–1263 (2020). doi:10.1126/science.abb2507 Medline

18. A. C. Walls, Y.-J. Park, M. A. Tortorici, A. Wall, A. T. McGuire, D. Veesler, Structure, function, and antigenicity of the SARS-CoV-2 spike glycoprotein. *Cell* S0092-8674(20)30262-2 (2020). doi:10.1016/j.cell.2020.02.058 Medline

19. Y. Yuan, D. Cao, Y. Zhang, J. Ma, J. Qi, Q. Wang, G. Lu, Y. Wu, J. Yan, Y. Shi, X. Zhang, G. F. Gao, Cryo-EM structures of MERS-CoV and SARS-CoV spike glycoproteins reveal the dynamic receptor binding domains. *Nat. Commun.* **8**, 15092 (2017). doi:10.1038/ncomms15092 Medline

20. M. Gui, W. Song, H. Zhou, J. Xu, S. Chen, Y. Xiang, X. Wang, Cryo-electron microscopy structures of the SARS-CoV spike glycoprotein reveal a prerequisite conformational state for receptor binding. *Cell Res.* **27**, 119–129 (2017). doi:10.1038/cr.2016.152 Medline

21. R. N. Kirchdoerfer, N. Wang, J. Pallesen, D. Wrapp, H. L. Turner, C. A. Cottrell, K. S. Corbett, B. S. Graham, J. S. McLellan, A. B. Ward, Stabilized coronavirus spikes are resistant to conformational changes induced by receptor recognition or proteolysis. *Sci. Rep.* **8**, 15701 (2018). doi:10.1038/s41598-018-34171-7 Medline

22. Yuan *et al*. (*19*) observed 56% of the wild-type recombinant SARS-CoV S protein particle in none-"up" conformation and 44% in single-"up" conformation, while Kirchdoerfer *et al*. (*21*) found that recombinant SARS-CoV S protein, with K968P/V969P mutations in the S2 subunit to stabilize the prefusion conformation, has 58% single-"up", 39% in double-"up", and 3% in triple-"up" conformations. However, it is not known whether the distribution of different configurations of S proteins on virus surface is the same as that of recombinant S protein.

23. S. Bangaru, S. Lang, M. Schotsaert, H. A. Vanderven, X. Zhu, N. Kose, R. Bombardi, J. A. Finn, S. J. Kent, P. Gilchuk, I. Gilchuk, H. L. Turner, A. García-Sastre, S. Li, A. B. Ward, I. A. Wilson, J. E. Crowe Jr., A site of vulnerability on the influenza virus hemagglutinin head domain trimer interface. *Cell* **177**, 1136–1152.e18 (2019). doi:10.1016/j.cell.2019.04.011 Medline

24. A. Watanabe, K. R. McCarthy, M. Kuraoka, A. G. Schmidt, Y. Adachi, T. Onodera, K. Tonouchi, T. M. Caradonna, G. Bajic, S. Song, C. E. McGee, G. D. Sempowski, F. Feng, P. Urick, T. B. Kepler, Y. Takahashi, S. C. Harrison, G. Kelsoe, Antibodies to a conserved influenza head interface epitope protect by an IgG subtype-dependent mechanism. *Cell* **177**, 1124–1135.e16 (2019). doi:10.1016/j.cell.2019.03.048 Medline

25. G. Bajic, M. J. Maron, Y. Adachi, T. Onodera, K. R. McCarthy, C. E. McGee, G. D. Sempowski, Y. Takahashi, G. Kelsoe, M. Kuraoka, A. G. Schmidt, Influenza antigen engineering focuses immune responses to a subdominant but broadly protective viral epitope. *Cell Host Microbe* **25**, 827–835.e6 (2019). doi:10.1016/j.chom.2019.04.003 Medline

26. J. Lee, D. R. Boutz, V. Chromikova, M. G. Joyce, C. Vollmers, K. Leung, A. P. Horton, B. J. DeKosky, C.-H. Lee, J. J. Lavinder, E. M. Murrin, C. Chrysostomou, K. H. Hoi, Y. Tsybovsky, P. V. Thomas, A. Druz, B. Zhang, Y. Zhang, L. Wang, W.-P. Kong, D. Park, L. I. Popova, C. L. Dekker, M. M. Davis, C. E. Carter, T. M. Ross, A. D. Ellington, P. C. Wilson, E. M. Marcotte, J. R. Mascola, G. C. Ippolito, F. Krammer, S. R. Quake, P. D. Kwong, G. Georgiou, Molecular-level analysis of the serum antibody repertoire in young adults before and after seasonal influenza vaccination. *Nat. Med.* **22**, 1456–1464 (2016). doi:10.1038/nm.4224 Medline

27. C. Dreyfus, N. S. Laursen, T. Kwaks, D. Zuijdgeest, R. Khayat, D. C. Ekiert, J. H. Lee, Z. Metlagel, M. V. Bujny, M. Jongeneelen, R. van der Vlugt, M. Lamrani, H.

J. W. M. Korse, E. Geelen, Ö. Sahin, M. Sieuwerts, J. P. J. Brakenhoff, R. Vogels, O. T. W. Li, L. L. M. Poon, M. Peiris, W. Koudstaal, A. B. Ward, I. A. Wilson, J. Goudsmit, R. H. E. Friesen, Highly conserved protective epitopes on influenza B viruses. *Science* **337**, 1343–1348 (2012). doi:10.1126/science.1222908 Medline

28. C. Petro, P. A. González, N. Cheshenko, T. Jandl, N. Khajoueinejad, A. Bénard, M. Sengupta, B. C. Herold, W. R. Jacobs Jr., Herpes simplex type 2 virus deleted in glycoprotein D protects against vaginal, skin and neural disease. *eLife* **4**, e06054 (2015). doi:10.7554/eLife.06054 Medline

29. A. Bootz, A. Karbach, J. Spindler, B. Kropff, N. Reuter, H. Sticht, T. H. Winkler, W. J. Britt, M. Mach, Protective capacity of neutralizing and non-neutralizing antibodies against glycoprotein B of cytomegalovirus. *PLOS Pathog.* **13**, e1006601 (2017). doi:10.1371/journal.ppat.1006601 Medline

30. C. W. Burke, J. W. Froude, S. Miethe, B. Hülseweh, M. Hust, P. J. Glass, Human-like neutralizing antibodies protect mice from aerosol exposure with western equine encephalitis virus. *Viruses* **10**, 147 (2018). doi:10.3390/v10040147 Medline

31. E. A. Henchal, L. S. Henchal, J. J. Schlesinger, Synergistic interactions of anti-NS1 monoclonal antibodies protect passively immunized mice from lethal challenge with dengue 2 virus. *J. Gen. Virol.* **69**, 2101–2107 (1988). doi:10.1099/0022-1317-69-8-2101 Medline

32. V. D. Menachery, B. L. Yount Jr., K. Debbink, S. Agnihothram, L. E. Gralinski, J. A. Plante, R. L. Graham, T. Scobey, X.-Y. Ge, E. F. Donaldson, S. H. Randell, A. Lanzavecchia, W. A. Marasco, Z.-L. Shi, R. S. Baric, A SARS-like cluster of circulating bat coronaviruses shows potential for human emergence. *Nat. Med.* **21**, 1508–1513 (2015). doi:10.1038/nm.3985 Medline

33. V. D. Menachery, B. L. Yount Jr., A. C. Sims, K. Debbink, S. S. Agnihothram, L. E. Gralinski, R. L. Graham, T. Scobey, J. A. Plante, S. R. Royal, J. Swanstrom, T. P. Sheahan, R. J. Pickles, D. Corti, S. H. Randell, A. Lanzavecchia, W. A. Marasco, R. S. Baric, SARS-like WIV1-CoV poised for human emergence. *Proc. Natl. Acad. Sci. U.S.A.* **113**, 3048–3053 (2016). doi:10.1073/pnas.1517719113 Medline

34. E. Krissinel, K. Henrick, Inference of macromolecular assemblies from crystalline state. *J. Mol. Biol.* **372**, 774–797 (2007). doi:10.1016/j.jmb.2007.05.022 Medline

35. J. E. Pak, C. Sharon, M. Satkunarajah, T. C. Auperin, C. M. Cameron, D. J. Kelvin, J. Seetharaman, A. Cochrane, F. A. Plummer, J. D. Berry, J. M. Rini, Structural insights into immune recognition of the severe acute respiratory syndrome coronavirus S protein receptor binding domain. *J. Mol. Biol.* **388**, 815–823 (2009). doi:10.1016/j.jmb.2009.03.042 Medline

36. W. C. Hwang, Y. Lin, E. Santelli, J. Sui, L. Jaroszewski, B. Stec, M. Farzan, W. A. Marasco, R. C. Liddington, Structural basis of neutralization by a human anti-severe acute respiratory syndrome spike protein antibody, 80R. *J. Biol. Chem.* **281**, 34610–34616 (2006). doi:10.1074/jbc.M603275200 Medline

37. D. C. Ekiert, R. H. E. Friesen, G. Bhabha, T. Kwaks, M. Jongeneelen, W. Yu, C. Ophorst, F. Cox, H. J. W. M. Korse, B. Brandenburg, R. Vogels, J. P. J. Brakenhoff, R. Kompier, M. H. Koldijk, L. A. H. M. Cornelissen, L. L. M. Poon, M. Peiris, W. Koudstaal, I. A. Wilson, J. Goudsmit, A highly conserved neutralizing epitope on group 2 influenza A viruses. *Science* **333**, 843–850 (2011). doi:10.1126/science.1204839 Medline

38. A. C. Walls, X. Xiong, Y.-J. Park, M. A. Tortorici, J. Snijder, J. Quispe, E. Cameroni, R. Gopal, M. Dai, A. Lanzavecchia, M. Zambon, F. A. Rey, D. Corti, D. Veesler, Unexpected receptor functional mimicry elucidates activation of coronavirus fusion. *Cell* **176**, 1026–1039.e15 (2019). doi:10.1016/j.cell.2018.12.028 Medline

39. Z. Otwinowski, W. Minor, Processing of X-ray diffraction data collected in oscillation mode. *Methods Enzymol.* **276**, 307–326 (1997). doi:10.1016/S0076-6879(97)76066-X

40. A. Teplyakov, J. Luo, G. Obmolova, T. J. Malia, R. Sweet, R. L. Stanfield, S. Kodangattil, J. C. Almagro, G. L. Gilliland, Antibody modeling assessment II. Structures and models. *Proteins* **82**, 1563–1582 (2014). doi:10.1002/prot.24554 Medline

41. F. Li, W. Li, M. Farzan, S. C. Harrison, Structure of SARS coronavirus spike receptor-binding domain complexed with receptor. *Science* **309**, 1864–1868 (2005). doi:10.1126/science.1116480 Medline

42. K. Arnold, L. Bordoli, J. Kopp, T. Schwede, The SWISS-MODEL workspace: A web-based environment for protein structure homology modelling. *Bioinformatics* **22**, 195–201 (2006). doi:10.1093/bioinformatics/bti770 Medline

43. P. Emsley, K. Cowtan, Coot: Model-building tools for molecular graphics. *Acta Crystallogr. D* **60**, 2126–2132 (2004). doi:10.1107/S0907444904019158 Medline

44. P. D. Adams, P. V. Afonine, G. Bunkóczi, V. B. Chen, I. W. Davis, N. Echols, J. J. Headd, L.-W. Hung, G. J. Kapral, R. W. Grosse-Kunstleve, A. J. McCoy, N. W. Moriarty, R. Oeffner, R. J. Read, D. C. Richardson, J. S. Richardson, T. C. Terwilliger, P. H. Zwart, PHENIX: A comprehensive Python-based system for macromolecular structure solution. *Acta Crystallogr. D* **66**, 213–221 (2010). doi:10.1107/S0907444909052925 Medline

45. N. C. Wu, G. Grande, H. L. Turner, A. B. Ward, J. Xie, R. A. Lerner, I. A. Wilson, In vitro evolution of an influenza broadly neutralizing antibody is modulated by hemagglutinin receptor specificity. *Nat. Commun.* **8**, 15371 (2017). doi:10.1038/ncomms15371 Medline

46. W. Song, M. Gui, X. Wang, Y. Xiang, Cryo-EM structure of the SARS coronavirus spike glycoprotein in complex with its host cell receptor ACE2. *PLOS Pathog.* **14**, e1007236 (2018). doi:10.1371/journal.ppat.1007236 Medline